Pt-Nb_2O_5-TiO_2 based semiconductors for photo-reforming of glucose and fructose aqueous solutions

Muhammad Umair[a], Marianna Bellardita[a,*], Giovanni Palmisano[b], Reem Al Sakkaf[b], Albin Pintar[c], Gregor Žerjav[c], Leonardo Palmisano[a], Vittorio Loddo[a]

[a]Department of Engineering, University of Palermo, Viale delle Scienze Building 6, 90127 Palermo, Italy

[b]Department of Chemical and Petroleum Engineering, Research and Innovation Center on CO_2 and Hydrogen (RICH), Khalifa University of Science and Technology, Abu Dhabi, United Arab Emirates

[c]Department of Inorganic Chemistry and Technology, National Institute of Chemistry, Hajdrihova 19, SI-1001 Ljubljana, Slovenia

Abstract - The conversion of biomass derivatives into fuels and valuable compounds under green conditions is increasingly attracting the attention of the scientific community. In this study, the photo-reforming of aqueous glucose and fructose solutions in the presence of 0.5 wt% Pt-loaded homemade bare and Nb_2O_5-TiO_2 catalysts was investigated to maximize the activity of titania for both hydrogen production and valuable chemical production. The samples were characterized by numerous surface and bulk techniques to discover a correlation between photoactivity and some catalyst properties. The most efficient sample was the home-prepared Pt-4%Nb_2O_5-HP, for both glucose and fructose conversion, with the highest H_2 productivity and the highest selectivity towards partially oxidized compounds. Photo-deposition of Pt was essential for H_2 production and, surprisingly, also increased the basicity of the TiO_2 surface; an

*Corresponding author. *E-mail address:* marianna.bellardita@unipa.it (Marianna Bellardita).

increase in surface acidity was measured when only niobium oxide was added, whereas stronger basic sites were observed in the simultaneous presence of Pt and niobium oxide.

Keywords: Photocatalysis, Selective biomass conversion, Nb_2O_5-TiO_2 catalysts, H_2 production

1. Introduction

Selective photo-reforming of biomass is an attractive and promising approach for the production of valuable chemicals and hydrogen [1,2]. Currently, biomasses can be converted into biofuels and chemicals by thermochemical and biological processes [3,4]. Thermochemical processes include pyrolysis, gasification, and liquefaction. However, these processes require drastic experimental conditions (high temperatures and pressures), the presence of harmful oxidants and/or toxic solvents, and a high energy input. In contrast, photo-reforming of biomass can be considered a “green” and low-cost technique. Indeed, the photocatalytic reactions are generally carried out under mild conditions (ambient temperature and pressure), often with water as solvent, using non-toxic semiconductors as photocatalysts, oxygen as oxidant, and sunlight or artificial light with low energy consumption as irradiation sources [5,6].

Given the problems caused by global warming and CO_2 emissions, the environmentally friendly production of H_2 is very important. Two routes can be taken to achieve this, one is the partial oxidation of non-renewable fossil fuels and the other is the processing of renewable energy resources, such as water or biomass. Biomass or biomass-derived compounds have the advantage of being renewable, easily transportable (solid or liquid), and having no impact in terms of CO_2 [7].

Glucose and its isomer fructose are derived from cellulose and can be used to produce high value-added products in a sustainable manner [8]. In particular, glucose can be converted to

ethanol, mannitol, and sorbitol by hydrogenation reactions [9], while 5-hydroxymethylfurfural (HMF) and hydrogen can be formed by dehydrogenation reactions [5,10,11]. In addition, gluconic and glucaric acids can be formed by partial oxidation reactions. The selective oxidation of glucose to gluconic, formic, levulinic, and lactic acids, as well as to arabinose and erythrose, is particularly attractive because they are industrially used platform chemicals [12]. In particular, gluconic acid and its derivatives are widely used in the pharmaceutical, detergent and food industries [13,14].

HMF is one of the 10 biological platform molecules with the highest added value that can be obtained from carbohydrates. Starting from HMF, it is possible to synthesize biofuels, polymer materials and fine chemicals [10]. HMF can be obtained from hexoses such as glucose and fructose by acid-catalyzed dehydration [10,11,15,16]. Fructose can be converted directly into HMF, whereas starting from glucose, an isomerization to fructose is required first and then its dehydration to HMF [17]. Solid acid catalysts with appropriate amount and strength of both Brønsted and Lewis acidic centers, such as Nb_2O_5, have been shown to be effective in converting glucose and fructose to HMF mainly through catalytic processes [10,11,15,18–21]. In addition, Nb_2O_5 is considered a water-tolerant solid acid and is therefore suitable for the dehydration of sugars in the aqueous phase via a catalytic route [22].

Titanium dioxide is widely used as a photocatalyst due to its low cost, high oxidizing power, virtually non-existent toxicity, low environmental impact, photostability, and high activity in partial oxidation reactions [23–25]. Datka et al. [26] reported the acidic properties of Nb_2O_5 on a variety of supports such as silica, alumina, titania and zirconia. Lewis acidity was measured in all niobium oxide support systems, while Brønsted acid sites were found only for niobium on alumina and silica. Few works investigated the use of Nb_2O_5/TiO_2 composites for the catalytic conversion of glucose or fructose into HMF [11,27]. Recently, the properties of niobium oxide were also investigated as a photocatalyst [16]. By coupling TiO_2 with niobium

oxide, it is possible to take advantage of the special electronic and surface properties of both photocatalysts and operate at ambient conditions. Nb_2O_5/TiO_2 heterojunctions showed higher activity than single oxides in the partial oxidation of α-phenylethanol and the photo-reforming of methanol [28], as well as in the photocatalytic degradation of rhodamine B [29].

In this work, homemade Nb_2O_5/TiO_2 photocatalysts containing niobia in various proportions and Pt (0.5 wt%) were prepared and used in a water suspension for the photo-reforming of glucose and fructose. The aim of this work was to modify the acidic surface properties of TiO_2 to improve the charge transfer process and enhance the performance of the composite photocatalysts for both the partial oxidation of sugars and simultaneous production of hydrogen. Different characterization techniques were used to link the photoactivity with some powder properties [30].

2. Experimental

2.1. Chemicals

Titanium tetrachloride (98%), hydrochloric acid (37%), ethanol, titanium(IV) isopropoxide (≥97%) named as TIP, niobium (V) chloride ($NbCl_5$), and Pluronic P127 were purchased from Sigma-Aldrich, whereas platinum chloride was obtained from BDH Chemicals and used for the synthesis of the various photocatalysts without further purification. Commercial sample P25 was also used as a reference and for comparison purposes.

2.2. Photocatalysts preparation

The sample given as HP was prepared by adding titanium(IV) isopropoxide (TIP) to an aqueous

solution containing HCl, Pluronic P127, and C_2H_5OH. The following molar ratios were used: TIP (1): H_2O (15): C_2H_5OH (40): HCl (0.5): P127 (0.005). The resulting solution was mixed at room temperature for about 4 h and then heated at 383 K overnight. The solid obtained was calcined at 773 K for 24 h.

The samples containing niobium were prepared by adding different amounts of $NbCl_5$ to the ethanolic solution before adding TIP. X% Nb-HP was the code used for these samples, where X% indicates the nominal weight percentage of Nb relative to TiO_2.

Some TiO_2 catalysts were loaded with 0.5 wt% Pt by a photo-deposition method. Distilled water (200 mL), ethanol (50 mL), $PtCl_4$ (5 mL), and the TiO_2 sample (1 g) were added to the photoreactor. The resulting mixture was stirred in the dark for 0.5 h with bubbling of He and then illuminated with a UV lamp (125 W) for 7 h. The resulting mixture was filtered, washed with distilled water, and then dried in an oven for 6 h.

2.3. Characterizations

X-ray diffraction (XRD) analyses of the prepared powders were performed with a Philips diffractometer (current 30 mA, voltage 40 kV) using CuKα radiation. UV-Vis diffuse reflectance spectra (DRS) were performed using a Shimadzu UV-2401 PC spectrophotometer with barium sulphate ($BaSO_4$) as reference material in the wavelength range of 200-800 nm at room temperature. These spectra allowed the band gap values of all photocatalysts to be determined by plotting the modified Kubelka-Munk function $[F(R'_\infty)hv]^{½}$ against the energy of the exciting light.

A Nova NanoSEM scanning electron microscope (SEM) was used to study the morphology of the solid samples. It was operated at 20 kV on samples on which a thin layer of gold had been vapour deposited. Specific surface area (SSA) was determined using a Flow Sorb 2300

instrument (Micromeritics) with the single-point BET method. Raman spectra of the samples were recorded using a BWTek-i-micro Raman Plus system equipped with a 785 nm diode laser. Photoluminescence (PL) spectra of the various solids were recorded using a Perkin Elmer LS55 fluorescence spectrometer in the 300-600 nm range with an excitation wavelength of 300 nm.

The DRIFTS spectra after pyridine adsorption were recorded using a Perkin Elmer Frontier FT-IR spectrometer equipped with a MCT (mercury cadmium telluride) detector. A sample was first heated in a N_2 stream from room temperature to 473 K and then held at this temperature for 15 minutes to clean the catalytic surface. Then the sample was cooled to 393 K and a background spectrum was recorded. Analyses were performed after the catalytic surface was saturated with pyridine for 20 minutes and the excess pyridine was then removed by purging with pure N_2.

A Malvern Panalytical zetasizer (model Ultra Red) equipped with a Malvern Multipurpose Titrator MPT-3 was used to measure zeta potential. 25 mg of a sample was dispersed in 100 mL of ultrapure water and stirred for 30 min (400 rpm). HCl (0.25 and 0.025 M) and NaOH (0.25 M) were used to control pH in the measurement range.

Thermogravimetric analysis (TGA) using pyridine as the probe molecule allowed determination of the acidic surface sites using a Perkin Elmer Pyris 1 TGA instrument. To clean the catalytic surface, samples were heated from 323 to 473 K and held at this temperature for 15 min. Then the samples were cooled to 393 K and pyridine was adsorbed until the weight of the catalyst was constant. Then the samples were purged with N_2 at 393 K to remove the excess pyridine. TPD (temperature-programmed desorption) profiles were determined in a temperature range from 393 to 773 K.

Basic surface sites were determined by TPD analyses using CO_2 as the probe molecule. The TPD profiles were obtained in a Micromeritics AutoChem II 2920 apparatus by heating the samples in a gas stream, O_2 (5%)/He (20 mL/min), for 10 minutes and cooling to 50 °C. Then

the gas flow was switched to Ar (20 mL/min) and CO_2 was introduced to the sample by metered pulses (80% by volume) in the Ar flow. Desorption of CO_2 from the sample was monitored in the temperature range of 50–360 °C (heating ramp 10 °C/min).

A Titan transmission electron microscope operating at 300 kV was used to perform transmission electron microscopy (TEM) measurements. Preparation of the samples consisted of suspending them in 2-propanol, ultrasonication of the obtained suspension, and applying 3 μL twice in succession to a 400-mesh Au grid (Tedpella). The solvent was then evaporated at room temperature. Using ImageJ, we were able to evaluate not only the distance d of the grating, but also how much the nanoparticles measured.

A Thermo Fisher Scientific (TFS) Escalab Xi+ XPS instrument equipped with an AlKα X-ray source was used for X-ray photoelectron spectroscopy (XPS) measurements. The top layer of the analyzed samples was cleaned of impurities by *in situ* etching with an Ar beam before performing the XPS measurements.

Electron paramagnetic resonance (EPR) spectra were recorded both to identify transition metal species and oxygen vacancies present in the solid photocatalysts and to identify the major free radicals involved in the photocatalytic process using an EMX-nano spectrometer (Bruker Biospin Corp., Karlsruhe, Germany). For the analysis of transition metal species and oxygen vacancies, the powder under investigation was placed in a tube that was inserted into the sample holder of the EPR test chamber for analysis. For the detection of superoxide anion radicals ($O_2^{\bullet-}$), the sample was instead suspended in methanol to form a 1 mg/mL suspension, which was then ultrasonically dispersed. A few drops of 100 mM of the scavenging agent 5,5-dimethyl-1-pyrroline-N-oxide (DMPO) were then added to the suspension. Similarly, detection of hydroxyl radicals ($OH^{\bullet}$) was performed by adding 100 μl of 1 mM H_2O_2 to the DMPO solution. The mixtures were mixed and placed in a test tube that was placed in the sample holder of the EPR test chamber for analysis. In all cases, analyses were performed by irradiating the samples with

a UV lamp (LOT -Quantum Design GmbH) for 30 min.

2.4. Photocatalytic reactions

Experiments were performed under anaerobic conditions with glucose or fructose as substrates at ambient temperature and pressure, monitoring the evolution of H_2 and CO_2 in the gas phase and the formation of the intermediates in the liquid phase. The photoreactor used was a cylindrical 800-mL Pyrex reactor, purged with helium for 30 min to reach the adsorption-desorption equilibrium of the substrate on the catalyst surface and to remove dissolved oxygen. Then the reactor was sealed and the near-UV lamp (125 W medium pressure Hg) was turned on. The initial concentration of the substrate was 1 mM and the pH of the solution was about 5 (the "natural" pH of the aqueous dispersions). A radiometer was used to determine the optimum amount of photocatalysts capable of absorbing about 90% of the photons emitted by the lamp. Specific amounts in the range of 0.5 g L^{-1} were determined for the different photocatalysts. Runs lasted 5 hours, and samples were collected at specific times and filtered through 2 µm membranes (HA, Millipore). A Thermo Scientific Dionex ultimate 3000 HPLC equipped with a Phenomenex REZEK ROA H^+ Organic acid column, diode array and refractive index detectors was used for the quantitative determination of glucose and fructose and the identification of their reaction products. An aqueous 2.5 mM H_2SO_4 solution with a flow rate of 0.6 mL min^{-1} was used as the eluent. The evolution of the gaseous species (H_2 and CO_2) during the runs was monitored by sampling 500 mL of gas from the reactor headspace at regular intervals and analyzing it using a HP 6890 series GC system equipped with a packed Supelco GC 60/80 CarboxenTM-1000 column and a thermal conductivity detector (TCD).

3. Results and discussion

3.1. Characterization of photocatalysts

Table 1 lists some physico-chemical properties of the photocatalysts used, such as the TiO_2 phases, band gap, specific surface areas, and isoelectric point (IEP) values of all the samples used. The commercially widely available TiO_2 P25 was chosen as the standard. The home-prepared samples, as well as the P25 sample, consist of a mixture of anatase and rutile, as shown by the XRD results (Fig. 1a). The S.S.A. of the home-prepared photocatalysts is higher than that of P25 and generally increases with increasing Nb_2O_5 content, with the highest value observed for the Pt-6% Nb_2O_5-HP sample.

Fig. 1a shows the XRD diffractograms of the prepared samples. Two major polymorphs of TiO_2, anatase and rutile, are present in all samples, indicating that the presence of Nb does not alter the crystalline structure of TiO_2. No peaks associated with the other constituents (Pt, Nb) can be seen, probably due to their small amount relative to TiO_2 and the high degree of dispersion. A close examination of the (101) peak of anatase (see Fig. 1a) shows a slight shift to lower angles in the presence of an increasing amount of Nb, which is due to the substitution of the Ti^{4+} ions of the TiO_2 lattice by Nb ions [31,32].

The Raman spectra of all samples (Fig. 1b) show the characteristic bands of anatase at 144 cm^{-1} (E_g), 197 cm^{-1} (E_g), 396 cm^{-1} (B_{1g}), 514 cm^{-1} (A_{1g}), and 637 cm^{-1} (B_{1g}) with high intensity, while the bands associated with rutile at 446 cm^{-1} and 613 cm^{-1} are not very clear because this polymorph is present in lower amounts than anatase. As noted in the XRD diffractograms, there are no identifiable peaks associated with Pt and Nb_2O_5 species. By magnifying the main anatase peak at 144 cm^{-1} (see Fig. 1b), a progressive shift to higher frequencies with increasing Nb_2O_5 content is visible compared to the Pt- HP sample. This can be attributed to the interaction of the

TiO_2 lattice with Nb, which causes the formation of oxygen vacancies instead of Ti^{4+} ions in agreement with the XRD results [31,33]. Moreover, the Raman spectra recorded in different areas of the samples are superimposable, indicating a homogeneous composition of samples.

Fig. 2 shows selected SEM micrographs of the semiconductors synthesized. All powders show irregular roundish particles with size in the range of 30-130 nm. Pt and Nb_2O_5 particles are indistinguishable, probably due to their small amount and uniform integration into the titanium dioxide matrix. After addition of the different amounts of niobium oxide, no differences in the morphology of the samples are observed.

Fig. 3 shows the UV-Vis diffuse reflectance spectra (DRS) of the different photocatalysts. All samples are active when irradiated with UV light and show a transition edge between 360 and 390 nm, which is typical for TiO_2-based semiconductors. Reflectance values of less than 50% in the visible range are due to the presence of photo-deposited Pt, which gives the powders a greyish colour [12]. The sample 4%Nb_2O_5-HP, which does not contain Pt, has a reflectance of over 90% in the same region. The band gaps of all photocatalysts were determined using the modified Kubelka-Munk function $[F(R'_\infty)h\nu]^{½}$ plotted against the energy of the exciting light; an example of the band gap estimation using this method is shown in Fig. 3. The Pt-TiO_2 based samples show similar band gap values between 2.99 and 3.09 eV.

Fig. 4 shows the results of the zeta potential measurements as a function of pH of the TiO_2-based composites. The isoelectric point (IEP), given in Table 1, is the pH at which the net charge on the catalyst surface is zero. The values vary from 3.67 to 5.00, with the highest value for the Pt-P25 solid and the lowest for the 4%Nb_2O_5-HP sample. The progressive decrease in IEP with the addition of Nb_2O_5 indicates an increase in the acidity of the surface of the composite samples. The low value of the 4%Nb_2O_5-HP sample, which does not contain Pt, indicates that Pt induces the formation of basic sites, the presence of which decreases the acidity of the surface. The differences measured in the other samples with different Nb_2O_5 content (recall that

the amount of Pt is 0.5 wt%, which is the same for all samples) are clearly due to the different amounts of oxide. Since the pH_{PZC} values of the photocatalysts are below 5 (approximately the value of the reacting solution), this means that the catalytic surface of all samples is negatively charged. However, since there are differences, even if they are not very large, Coulombic interactions of different magnitudes can occur, affecting the photoactivity between the species in the reaction mixture and the surface of the different photocatalysts [34].

Fig. 5 shows the solid-state photoluminescence spectra of the samples. The intensity of the spectra results from both the recombination of electron-hole pairs (the lower the intensity, the lower the recombination) and the presence of lattice defects or oxygen vacancies (the higher the intensity, the greater their number) [35,36]. The shape of the spectra is the same for all samples, indicating that the addition of foreign species to TiO_2 does not induce new emission phenomena. It is also noted that the presence of Pt decreases the intensity of PL compared to bare TiO_2, indicating a decrease in the recombination rate of photogenerated electron/hole pairs [32,35]. This leads to an improvement in the performance of Pt-TiO_2 compared to bare TiO_2 [37]. When only Nb_2O_5 is present, a slight increase in PL intensity is observed, which is due to the presence of oxygen vacancies. When both Pt and niobia are present, a progressive decrease in photoluminescence is observed as the percentage of Nb_2O_5 is increased. This may be due to both a decrease in the recombination rate and the formation of oxygen vacancies. For all samples, the main emission band is around 423 nm and can be attributed to the indirect band-to-band transition of electrons in TiO_2 in agreement with the band gap values. Signals at higher wavelengths can be attributed to the non-radiative recombination of excited electrons in lattice defects [38].

The investigation of the basic surface properties of the different catalysts was carried out after CO_2 adsorption on the TiO_2 surface using the TPD technique. Fig. 6 shows the CO_2-TPD profiles of the photocatalysts used and Table 2 gives the amounts of basic sites. The peak

between 50-150 °C could be attributed to the desorption of molecular CO_2, while the peak at temperatures around 300-350 °C is due to HCO_3^- or carboxylate originating from the interaction of CO_2 with the hydroxyl groups of the TiO_2 surface [39]. The presence of peaks at temperatures above 400 °C indicates stronger adsorption of CO_2 onto the solid; the samples containing contemporary Pt and Nb_2O_5 have stronger basic sites. The results presented in Table 2 show that the bare TiO_2 has the lowest number of basic sites, and that the presence of the noble metal or the niobium oxide significantly increases this number. A more pronounced effect is observed when both foreign species (Pt and Nb_2O_5) are present, and the higher the percentage of Nb_2O_5, the greater the number of basic sites, while the amount of Pt remains constant. This synergistic result is surprising, since it is commonly reported in the literature that the presence of Pt on TiO_2 only enhances the separation of photogenerated charges, while the coupling of Nb_2O_5 with TiO_2 causes an increase in the acidity of the host [11].

In situ diffuse reflectance infrared Fourier transform spectroscopy (DRIFTS) in the presence of adsorbed pyridine was used to determine the nature and density of acid sites on the surface as a function of the amount of Nb_2O_5. Fig. 7 shows the spectra of the different TiO_2 HP samples. The bands at 1445 cm^{-1}, 1486 cm^{-1}, 1574 cm^{-1} and 1604 cm^{-1} are characteristic of the pyridine ring coordinated to the Lewis acid sites on the surface, while the bands at 1545 cm^{-1} and 1635 cm^{-1} correspond to the pyridinium ions adsorbed on the Brønsted acid sites [40–44]. All samples show a clear predominance of Lewis acid sites, and although these spectra provide essentially qualitative information, it can be said with good approximation that the intensity is related to the concentration of the acid sites. Bare TiO_2 HP shows intense and sharp peaks, the reduction of which can be detected after Pt photo-deposition (see Pt-HP sample), in agreement with the CO_2 TPD results. This confirms that the presence of Pt not only affects the separation of electrons and holes, but also the acidity of the surface. The sole presence of Nb_2O_5 increases the acidity of the TiO_2 surface, with the sample 4%Nb_2O_5-HP showing the most intense peaks,

but no new peaks are present. In the simultaneous presence of Pt and niobium oxide, the intensity of the peaks is slightly higher at higher Nb_2O_5 contents than at pure TiO_2, while a slight change (appearance of a broad band) is observed in the spectrum around 1525 cm^{-1}. This effect is more pronounced for samples with a higher Nb_2O_5 content.

The amount and density of acidic sites were determined by pyridine TPD measurements. Fig. 8 shows the TPD pyridine curves of the tested materials, and Table 3 gives the amount and density of acid sites on the catalytic surface along with the temperature of pyridine desorption. The addition of Pt decreases the density of acid sites, while Nb_2O_5 generally has an opposite effect. In the simultaneous presence of the two components, no significant changes in the total amount of acid sites are observed compared to bare TiO_2 due to their opposite behaviour. In any case, the addition of foreign species leads to an increase in the pyridine desorption temperature, indicating an increase in the strength of the acid sites.

Fig. 9 shows TEM images of samples Pt-HP and Pt-6%Nb_2O_5-HP. In the last sample, unfortunately, it was not possible to distinguish the Pt from niobia particles. In the Pt-HP sample Pt nanoparticles (represented by small dark spheres) are concentrated in some areas of the TiO_2 surface. The size of Pt nanoparticles ranges from 5 to 25 nm; when the image is enlarged, two lattice fringes of about 0.35 nm and 0.32 nm can be seen, which are characteristic of the (1 0 1) anatase and (1 1 0) rutile planes, respectively [45].

In the XPS survey spectrum (not given for brevity), peaks for Ti, O, and Cl (as residues of HCl, $PtCl_4$, and $NbCl_5$ precursors) were detected in all samples. Peaks for Pt and Nb were rarely detected because of their low atomic concentration. When both are present, Cl and Nb are not clearly distinguishable because their peaks almost overlap.

Fig. 10a shows the high-resolution XPS spectra of the Ti 2p peaks. The two peaks of Ti $2p_{3/2}$ at 459.5 eV and Ti $2p_{1/2}$ at 465.3 eV with a binding energy gap of 5.8 eV are characteristic of Ti^{4+} in TiO_2 [46]. The high-resolution O 1s spectra are shown in Fig. 10b. For both samples, the

main peak is the one at about 530.7 eV, which is assigned to the O^{2-} ions of the TiO_2 crystal lattice. In the presence of Nb_2O_5, the peaks are at ca. 532 eV and at ca. 533.0 eV, which are related (in agreement with Raman spectra) to oxygen vacancies in TiO_2 [47] and -OH groups [48], respectively. In Fig. 10c, the main Pt peak at about 76 eV corresponds to Pt^0, and the less intense peaks at lower binding energy visible in the sample Pt-6%Nb_2O_5-HP are characteristic of partially oxidized Pt species [49]. Moreover, the peaks for Pt in the Pt-6%Nb_2O_5-HP sample are much more intense, indicating a higher atomic concentration of Pt in this sample. As can be seen in Fig. 10d, no peaks were detected for Nb (the two peaks characteristic of Nb_2O_5 are at 209.9 eV and 207.1 eV [28]), which is probably due to the low atomic concentration. The small broad peak at lower binding energy is that of Cl 2p, the chlorine present in the precursor of Nb_2O_5.

The EPR spectra of the powder samples (Fig. 11a) show no EPR signal, indicating that the photocatalysts cannot generate free electrons and oxygen vacancies under illumination. In the presence of H_2O/DMPO/MeOH solution (Fig. 11b), no EPR signal can be detected in the experiments performed in the dark, indicating that the photocatalysts cannot generate radicals in the absence of illumination. When the photocatalysts are irradiated, the EPR spectra show the characteristic paramagnetic resonance absorption of the DMPO-$^{\bullet}O_2^-$ adduct [50]. This result indicates that both photocatalysts can thermodynamically generate superoxide anion radicals ($^{\bullet}O_2^-$) under illumination. The EPR spectrum of the Pt-6%Nb_2O_5-HP sample shows higher intensity peaks, indicating stronger formation of the oxygen radicals, which is probably due to the more effective charge separation in the presence of Nb_2O_5. For Pt-HP samples suspended in water in the dark and in the presence of DMPO and H_2O_2 (Fig. 11c), no EPR signals are detected, while the signals just mentioned are visible in the presence of Nb_2O_5. Upon irradiation, the EPR spectra lead to the characteristic paramagnetic resonance absorption of the

DMPO-•OH adduct only for the sample Pt-6%Nb_2O_5-HP. Therefore, only this sample can thermodynamically generate hydroxyl radicals (•OH) under illumination.

3.2. Photocatalytic results

All TiO_2-based photocatalysts were used for the photo-reforming of aqueous glucose and fructose solutions under irradiation with near-UV light under anaerobic conditions. The obtained results were compared to relate the reactivity to some catalyst features. The presence of Pt nanoparticles on the catalyst surface increased the photoactivity thanks to their role in reducing the recombination rate of photogenerated e^-/h^+ pairs (in agreement with the results of solid-state PL analysis) and was essential for H_2 production, since in its absence only compounds from partial oxidation of the starting substrates and CO_2 from mineralization were observed (Tables 4 and 5). The different samples showed different conversions for both substrates, and the main partial oxidation products in the liquid phase were gluconic acid, arabinose, formic acid, erythrose, and fructose. In addition, H_2 and CO_2 were found in the gas phase in the headspace of the photoreactor.

Fig. 12 shows the concentration values of the two substrates and their intermediates as a function of irradiation time for the series of experiments performed with the different Nb_2O_5-modified photocatalysts. All catalysts produced the same compounds, suggesting very similar reaction mechanisms [12]; only a different degree of conversion, amount of the intermediates and H_2 production were observed for the different photocatalysts for both substrates. The different activity of the photocatalysts used depended on the electronic and physico-chemical properties of the different TiO_2-based solids, such as the recombination rate of the photogenerated charges, the acidity and/or basicity of the surface, the number of active sites per surface unit (a parameter also related to the specific surface area) and so on. When the substrate

was glucose, fructose was formed by isomerization, and both could form gluconic acid by oxidation of the anomeric C1 centre, converting the aldehyde group to the carboxyl group. A parallel mechanism consisted of α-cleavage, in which arabinose was formed in the first step and erythrose together with formic acid and hydrogen in the second step [12,51].

Tables 4 and 5 show the conversion, selectivity, and amounts of H_2 and CO_2 for the runs starting from glucose and fructose, respectively, using the different photocatalysts. In particular, it has been shown that a Pt-P25 sample used for comparison purposes generally performs less well than some HP-modified samples (with Pt and Nb_2O_5). The Pt-HP catalyst showed good conversion and selectivity towards arabinose with both glucose and fructose as starting substrates. Starting from glucose, the highest conversion was obtained with the sample Pt-2%Nb_2O_5-HP, while a lower degree of conversion was observed in the exclusive presence of Nb_2O_5, suggesting that the surface acidity (the sample 4%Nb_2O_5-HP showed the most intense DRIFT peaks in the presence of adsorbed pyridine) had an adverse effect. In this case, the increased amount of superoxide and hydroxyl radicals in the Nb_2O_5-containing samples (see EPR results) had no positive effect on the oxidation capacity of TiO_2. Fructose was formed practically only with the Pt-HP sample, since the increase in surface basicity (Table 2) due to the simultaneous presence of Pt and Nb_2O_5 was detrimental to the isomerization of glucose to fructose, in agreement with the literature [52]. The selectivity towards arabinose was favoured by Nb_2O_5, and in agreement with the α-cleavage mechanism, practically almost the same amount of arabinose and formic acid were obtained [12,51]. Starting from fructose, low amounts of Nb_2O_5 had no significant effect on the degree of conversion, while the highest amounts had a negative effect. Moreover, the lowest amounts of Nb_2O_5 favoured the formation of arabinose.

The best photocatalyst for H_2 production under the operating and reaction conditions used was Pt-4%Nb_2O_5-HP in the presence of both substrates. The trend in terms of Nb_2O_5 content increased up to 4%, then H_2 production decreased.

4. Conclusions

0.5 wt% Pt loaded home-prepared bare and Nb_2O_5-TiO_2 photocatalysts with different Nb_2O_5 content were prepared to evaluate their activity in the reforming of glucose and fructose. The photocatalytic results confirm that the photoactivity does not depend on a single parameter but is a compromise between several factors. The sample Pt-2%Nb_2O_5-HP proved to be the most oxidizing catalyst, but the solid Pt-4%Nb_2O_5-HP was the most powerful in terms of partial oxidation products and H_2 formation. Neither sample exhibited a property that could affect either type of photoactivity relative to the other, but had intermediate values for PZC, number of basic sites, oxygen vacancies, and photoluminescence effects (see PL spectra).

The samples were characterized using different techniques to investigate the effects of Pt and Nb_2O_5 on the properties of the catalyst. Pt not only acted as an electron sink and improved the efficiency of e^-/h^+ separation, as reported in the literature, but surprisingly also changed the acid-base properties of the surface by increasing the number of basic sites. Nb_2O_5 alone increased the acidity of the TiO_2 surface, while stronger basic sites were formed compared to the bare host when Pt was also present. The increase in surface basicity due to the simultaneous presence of Pt and Nb_2O_5 adversely affected the isomerization of glucose to fructose. The formation of $^{\bullet}O_2^-$ and $^{\bullet}OH$ radicals in the samples containing Nb_2O_5 did not have a positive effect on the oxidizing power of TiO_2, but favoured partial oxidation reactions and the formation of H_2. The home-prepared samples outperformed the well-known commercial TiO_2 P25.

Declaration of competing interest - The authors declare that they have no known competing financial interests or personal relationships that could have appeared to influence the work reported in this paper.

Acknowledgments - AP and GŽ acknowledge the financial support from the Slovenian Research and Innovation Agency (research core funding No. P2-0150). GP acknowledge Dr. Thomas Delclos for XPS analysis and Dr. Samar B. Al Jitan for experimental support. The Research and Innovation Center on CO_2 and Hydrogen (RICH) at Khalifa University is acknowledged for infrastructure and equipment.

Data availability - Data will be made available on request.

References

[1] U. Nwosu, A. Wang, B. Palma, H. Zhao, M.A. Khan, M. Kibria, J. Hu, Selective biomass photoreforming for valuable chemicals and fuels: A critical review, Renewable and Sustainable Energy Reviews. 148 (2021) 111266. https://doi.org/10.1016/J.RSER.2021.111266.

[2] C.M. Pecoraro, M. Bellardita, V. Loddo, D. Virtù, F. Di Franco, M. Santamaria, Photocatalytic and photoelectrocatalytic H2 evolution combined with valuable furfural production, Appl Catal A Gen. 650 (2023). https://doi.org/10.1016/j.apcata.2022.118987.

[3] R. Sindhu, P. Binod, A. Pandey, Biological pretreatment of lignocellulosic biomass – An overview, Bioresour Technol. 199 (2016) 76–82. https://doi.org/10.1016/J.BIORTECH.2015.08.030.

[4] L. Zhang, C. (Charles) Xu, P. Champagne, Overview of recent advances in thermo-chemical conversion of biomass, Energy Convers Manag. 51 (2010) 969–982. https://doi.org/10.1016/J.ENCONMAN.2009.11.038.

[5] M. Bellardita, V. Loddo, L. Palmisano, Formation of High Added Value Chemicals by Photocatalytic Treatment of Biomass, Mini Rev Org Chem. 17 (2020) 884–901. https://doi.org/10.2174/1570193x17666200131112856.

[6] L. Palmisano, V. Augugliaro, M. Bellardita, A. Di Paola, E. García López, V. Loddo, G. Marcì, G. Palmisano, S. Yurdakal, Titania photocatalysts for selective oxidations in water, ChemSusChem. 4 (2011) 1431–1438. https://doi.org/10.1002/cssc.201100196.

[7] M. Ni, D.Y.C. Leung, M.K.H. Leung, K. Sumathy, An overview of hydrogen production from biomass, Fuel Processing Technology. 87 (2006) 461–472. https://doi.org/10.1016/J.FUPROC.2005.11.003.

[8] F.W. Lichtenthaler, S. Peters, Carbohydrates as green raw materials for the chemical industry, Comptes Rendus Chimie. 7 (2004) 65–90. https://doi.org/10.1016/j.crci.2004.02.002.

[9] B. García, J. Moreno, G. Morales, J.A. Melero, J. Iglesias, Production of sorbitol via catalytic transfer hydrogenation of Glucose, Applied Sciences (Switzerland). 10 (2020). https://doi.org/10.3390/app10051843.

[10] M.N. Catrinck, E.S. Ribeiro, R.S. Monteiro, R.M. Ribas, M.H.P. Barbosa, R.F. Teófilo, Direct conversion of glucose to 5-hydroxymethylfurfural using a mixture of niobic acid and niobium phosphate as a solid acid catalyst, Fuel. 210 (2017) 67–74. https://doi.org/10.1016/j.fuel.2017.08.035.

[11] F. Huang, T. Jiang, X. Xu, L. Chen, G. Laurenczy, Z. Fei, P.J. Dyson, A TiO2/Nb2O5·: N H2O heterojunction catalyst for conversion of glucose into 5-hydroxymethylfurfural in water, Catal Sci Technol. 10 (2020) 7857–7864. https://doi.org/10.1039/d0cy01601b.

[12] M. Bellardita, E.I. García-López, G. Marcì, L. Palmisano, Photocatalytic formation of H2 and value-added chemicals in aqueous glucose (Pt)-TiO2 suspension, Int J Hydrogen Energy. 41 (2016) 5934–5947. https://doi.org/10.1016/j.ijhydene.2016.02.103.

[13] S. Ramachandran, P. Fontanille, A. Pandey, C. Larroche, Gluconic Acid: Properties, Applications and Microbial Production, (n.d.).

[14] E.F. Bernstein, D.B. Brown, M.D. Schwartz, K. Kaidbey, S.M. Ksenzenko, Z.D. Draelos, The Polyhydroxy Acid Gluconolactone Protects Against Ultraviolet Radiation in an In Vitro Model of Cutaneous, Dermatologic Surgery. 30 (2004) 189–196. https://doi.org/10.1111/j.1524-4725.2004.30060.x.

[15] M. Marzo, A. Gervasini, P. Carniti, Improving stability of Nb 2O 5 catalyst in fructose dehydration reaction in water solvent by ion-doping, in: Catal Today, 2012: pp. 89–95. https://doi.org/10.1016/j.cattod.2011.12.014.

[16] K. Su, H. Liu, Z. Gao, P. Fornasiero, F. Wang, Nb2O5-Based Photocatalysts, Advanced Science. 8 (2021). https://doi.org/10.1002/advs.202003156.

[17] Y. Román-Leshkov, M. Moliner, J.A. Labinger, M.E. Davis, Mechanism of glucose isomerization using a solid lewis acid catalyst in water, Angewandte Chemie - International Edition. 49 (2010) 8954–8957. https://doi.org/10.1002/anie.201004689.

[18] R. Weingarten, G.A. Tompsett, W.C. Conner, G.W. Huber, Design of solid acid catalysts for aqueous-phase dehydration of carbohydrates: The role of Lewis and Brønsted acid sites, J Catal. 279 (2011) 174–182. https://doi.org/10.1016/j.jcat.2011.01.013.

[19] X. Qi, M. Watanabe, T.M. Aida, R.L. Smith, Catalytical conversion of fructose and glucose into 5-hydroxymethylfurfural in hot compressed water by microwave heating, Catal Commun. 9 (2008) 2244–2249. https://doi.org/10.1016/j.catcom.2008.04.025.

[20] I. Agirrezabal-Telleria, C. García-Sancho, P. Maireles-Torres, P.L. Arias, Dehydration of xylose to furfural using a Lewis or Brönsted acid catalyst and N2 stripping, Cuihua Xuebao/Chinese Journal of Catalysis. 34 (2013) 1402–1406. https://doi.org/10.1016/s1872-2067(12)60599-3.

[21] M. Watanabe, Y. Aizawa, T. Iida, R. Nishimura, H. Inomata, Catalytic glucose and fructose conversions with TiO2 and ZrO2 in water at 473 K: Relationship between reactivity and acid-base property determined by TPD measurement, Appl Catal A Gen. 295 (2005) 150–156. https://doi.org/10.1016/j.apcata.2005.08.007.

[22] M.T. Reche, A. Osatiashtiani, L.J. Durndell, M.A. Isaacs, Â. Silva, A.F. Lee, K. Wilson, Niobic acid nanoparticle catalysts for the aqueous phase transformation of glucose and fructose to 5-hydroxymethylfurfural, Catal Sci Technol. 6 (2016) 7334–7341. https://doi.org/10.1039/c6cy01129b.

[23] M.A. Henderson, A surface science perspective on TiO2 photocatalysis, Surf Sci Rep. 66 (2011) 185–297. https://doi.org/10.1016/j.surfrep.2011.01.001.

[24] A. Fujishima, T.N. Rao, D.A. Tryk, Titanium dioxide photocatalysis, 2000.

[25] M. Pelaez, N.T. Nolan, S.C. Pillai, M.K. Seery, P. Falaras, A.G. Kontos, P.S.M. Dunlop, J.W.J. Hamilton, J.A. Byrne, K. O'Shea, M.H. Entezari, D.D. Dionysiou, A review on the visible light active titanium dioxide photocatalysts for environmental applications, Appl Catal B. 125 (2012) 331–349. https://doi.org/10.1016/j.apcatb.2012.05.036.

[26] J. Datka, A.M. Turek, J.M. Jehng, I.E. Wachs, Acidic Properties of Supported Niobium Oxide Catalysts: An Infrared Spectroscopy Investigation, 1992.

[27] D. Stošić, S. Bennici, V. Pavlović, V. Rakić, A. Auroux, Tuning the acidity of niobia: Characterization and catalytic activity of Nb2O5-MeO2 (Me = Ti, Zr, Ce) mesoporous mixed oxides, Mater Chem Phys. 146 (2014) 337–345. https://doi.org/10.1016/j.matchemphys.2014.03.033.

[28] J. Yan, G. Wu, N. Guan, L. Li, Nb2O5/TiO2 heterojunctions: Synthesis strategy and photocatalytic activity, Appl Catal B. 152–153 (2014) 280–288. https://doi.org/10.1016/j.apcatb.2014.01.049.

[29] C.L. Ücker, F. Riemke, V. Goetzke, M.L. Moreira, C.W. Raubach, E. Longo, S. Cava, Facile preparation of Nb2O5/TiO2 heterostructures for photocatalytic application, Chemical Physics Impact. 4 (2022). https://doi.org/10.1016/j.chphi.2022.100079.

[30] M. Bellardita, M. Feilizadeh, R. Fiorenza, S. Scirè, L. Palmisano, V. Loddo, Selective aqueous oxidation of aromatic alcohols under solar light in the presence of TiO2 modified with different metal species, Photochemical and Photobiological Sciences. (2022). https://doi.org/10.1007/s43630-022-00284-2.

[31] B. Choudhury, B. Borah, A. Choudhury, Ce-Nd codoping effect on the structural and optical properties of TiO 2 nanoparticles, Mater Sci Eng B Solid State Mater Adv Technol. 178 (2013) 239–247. https://doi.org/10.1016/j.mseb.2012.11.017.

[32] R. Fiorenza, M. Bellardita, S. Scirè, L. Palmisano, Effect of the addition of different doping agents on visible light activity of porous TiO2 photocatalysts, Molecular Catalysis. 455 (2018) 108–120. https://doi.org/10.1016/j.mcat.2018.06.002.

[33] J.C. Parker, R.W. Siegel, Calibration of the Raman spectrum to the oxygen stoichiometry of nanophase TiO2, Appl Phys Lett. 57 (1990) 943–945. https://doi.org/10.1063/1.104274.

[34] D. Maučec, A. Šuligoj, A. Ristić, G. Dražić, A. Pintar, N.N. Tušar, Titania versus zinc oxide nanoparticles on mesoporous silica supports as photocatalysts for removal of dyes from wastewater at neutral pH, Catal Today. 310 (2018) 32–41. https://doi.org/10.1016/j.cattod.2017.05.061.

[35] A. Di Paola, M. Bellardita, G. Marc, L. Palmisano, F. Parrino, R. Amadelli, Preparation of Sm-loaded brookite TiO2 photocatalysts, Catal Today. 161 (2011) 35–40. https://doi.org/10.1016/j.cattod.2010.11.016.

[36] J. Liqiang, S. Xiaojun, X. Baifu, W. Baiqi, C. Weimin, F. Honggang, The preparation and characterization of la doped TiO2 nanoparticles and their photocatalytic activity, J Solid State Chem. 177 (2004) 3375–3382. https://doi.org/10.1016/j.jssc.2004.05.064.

[37] S. Al Jitan, Y. Li, D. Bahamon, G. Žerjav, V.S. Tatiparthi, C. Aubry, M. Sinnokrot, Z. Matouk, N. Rajput, M. Gutierrez, K. Al-Ali, R. Hashaikeh, A. Pintar, L.F. Vega, G. Palmisano, Unprecedented photocatalytic conversion of gaseous and liquid CO2 on graphene-impregnated Pt/Cu-TiO2: The critical role of Cu dopant, J Environ Chem Eng. 11 (2023). https://doi.org/10.1016/j.jece.2023.109485.

[38] N.D. Abazović, M.I. Čomor, M.D. Dramićanin, D.J. Jovanović, S.P. Ahrenkiel, J.M. Nedeljković, Photoluminescence of anatase and rutile TiO2 particles, Journal of Physical Chemistry B. 110 (2006) 25366–25370. https://doi.org/10.1021/jp064454f.

[39] J. Zhao, Y. Wang, Y. Li, X. Yue, C. Wang, Phase-dependent enhancement for CO2 photocatalytic reduction over CeO2/TiO2 catalysts, Catal Sci Technol. 6 (2016) 7967–7975. https://doi.org/10.1039/c6cy01365a.

[40] S. Songtawee, B. Rungtaweevoranit, C. Klaysom, K. Faungnawakij, Tuning Brønsted and Lewis acidity on phosphated titanium dioxides for efficient conversion of glucose to 5-hydroxymethylfurfural, RSC Adv. 11 (2021) 29196–29206. https://doi.org/10.1039/d1ra06002c.

[41] V.V. Kumar, G. Naresh, S. Deepa, P.G. Bhavani, M. Nagaraju, M. Sudhakar, K.V.R. Chary, A. Venugopal, J. Tardio, S.K. Bhargava, Influence of W on the reduction behaviour and Brønsted acidity of Ni/TiO2 catalyst in the hydrogenation of levulinic acid to valeric acid: Pyridine adsorbed DRIFTS study, Appl Catal A Gen. 531 (2017) 169–176. https://doi.org/10.1016/J.APCATA.2016.10.032.

[42] M. Addamo, M. Del Arco, M. Bellardita, D. Carriazo, A. Di Paola, E. García-López, G. Marcì, C. Martín, L. Palmisano, V. Rives, Photoactivity of nanostructured TiO 2 catalysts in aqueous system and their surface acid-base, bulk and textural properties, 2007. www.brill.nl/rci.

[43] M.I. Zaki, M.A. Hasan, F.A. Al-Sagheer, L. Pasupulety, In situ FTIR spectra of pyridine adsorbed on SiO2–Al2O3, TiO2, ZrO2 and CeO2: general considerations for the identification of acid

sites on surfaces of finely divided metal oxides, Colloids Surf A Physicochem Eng Asp. 190 (2001) 261–274. https://doi.org/10.1016/S0927-7757(01)00690-2.

[44] L. Ding, M. Li, Y. Zhao, H. Zhang, J. Shang, J. Zhong, H. Sheng, C. Chen, J. Zhao, The vital role of surface Brönsted acid/base sites for the photocatalytic formation of free ·OH radicals, Appl Catal B. 266 (2020). https://doi.org/10.1016/j.apcatb.2020.118634.

[45] F. Xu, W. Xiao, B. Cheng, J. Yu, Direct Z-scheme anatase/rutile bi-phase nanocomposite TiO2 nanofiber photocatalyst with enhanced photocatalytic H2-production activity, Int J Hydrogen Energy. 39 (2014) 15394–15402. https://doi.org/10.1016/j.ijhydene.2014.07.166.

[46] T. Jedsukontorn, T. Ueno, N. Saito, M. Hunsom, Facile preparation of defective black TiO2 through the solution plasma process: Effect of parametric changes for plasma discharge on its structural and optical properties, J Alloys Compd. 726 (2017) 567–577. https://doi.org/10.1016/j.jallcom.2017.08.028.

[47] T. Jedsukontorn, T. Ueno, N. Saito, M. Hunsom, Facile preparation of defective black TiO2 through the solution plasma process: Effect of parametric changes for plasma discharge on its structural and optical properties, J Alloys Compd. 726 (2017) 567–577. https://doi.org/10.1016/j.jallcom.2017.08.028.

[48] M. Bellardita, C. Garlisi, A.M. Venezia, G. Palmisano, L. Palmisano, Influence of fluorine on the synthesis of anatase TiO2 for photocatalytic partial oxidation: Are exposed facets the main actors?, Catal Sci Technol. 8 (2018) 1606–1620. https://doi.org/10.1039/c7cy02382k.

[49] J.J. Murcia, M.C. Hidalgo, J.A. Navío, V. Vaiano, P. Ciambelli, D. Sannino, Photocatalytic ethanol oxidative dehydrogenation over Pt/TiO2: Effect of the addition of blue phosphors, International Journal of Photoenergy. 2012 (2012). https://doi.org/10.1155/2012/687262.

[50] W. He, Y. Liu, W.G. Wamer, J.J. Yin, Electron spin resonance spectroscopy for the study of nanomaterial-mediated generation of reactive oxygen species, J Food Drug Anal. 22 (2014) 49–63. https://doi.org/10.1016/j.jfda.2014.01.004.

[51] R. Chong, J. Li, Y. Ma, B. Zhang, H. Han, C. Li, Selective conversion of aqueous glucose to value-added sugar aldose on TiO2-based photocatalysts, J Catal. 314 (2014) 101–108. https://doi.org/10.1016/j.jcat.2014.03.009.

[52] S. Songtawee, B. Rungtaweevoranit, C. Klaysom, K. Faungnawakij, Tuning Brønsted and Lewis acidity on phosphated titanium dioxides for efficient conversion of glucose to 5-hydroxymethylfurfural, RSC Adv. 11 (2021) 29196–29206. https://doi.org/10.1039/d1ra06002c.

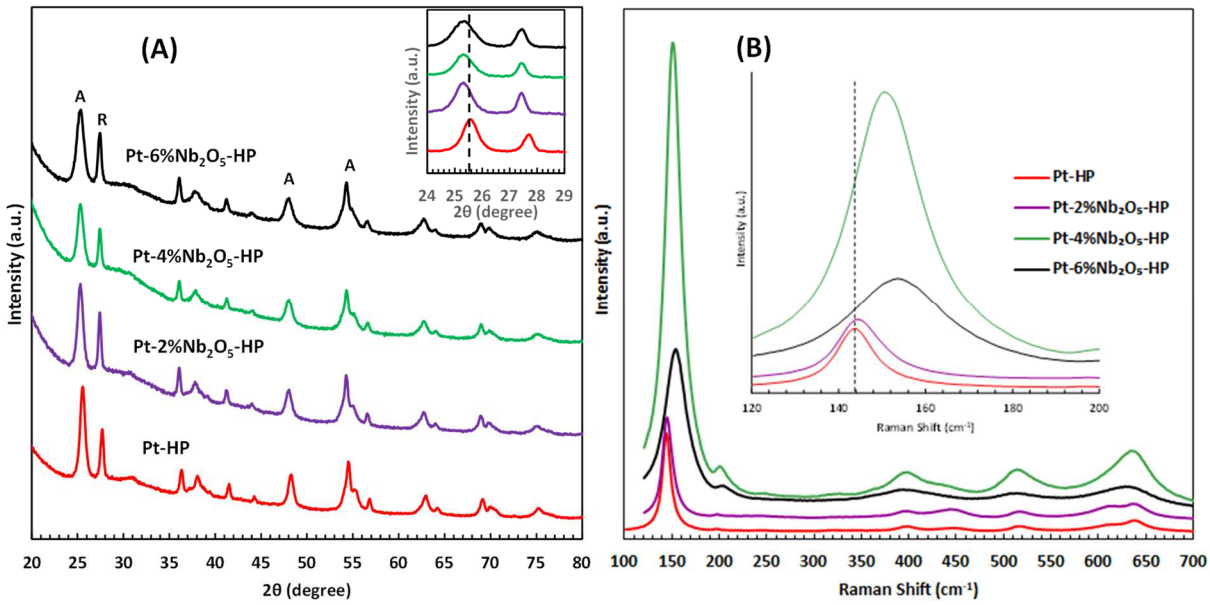

Fig. 1. XRD patterns (A) and Raman spectra (B) of Pt-HP, Pt-2%Nb_2O_5-HP, Pt-4%Nb_2O_5-HP and Pt-6%Nb_2O_5-HP samples.

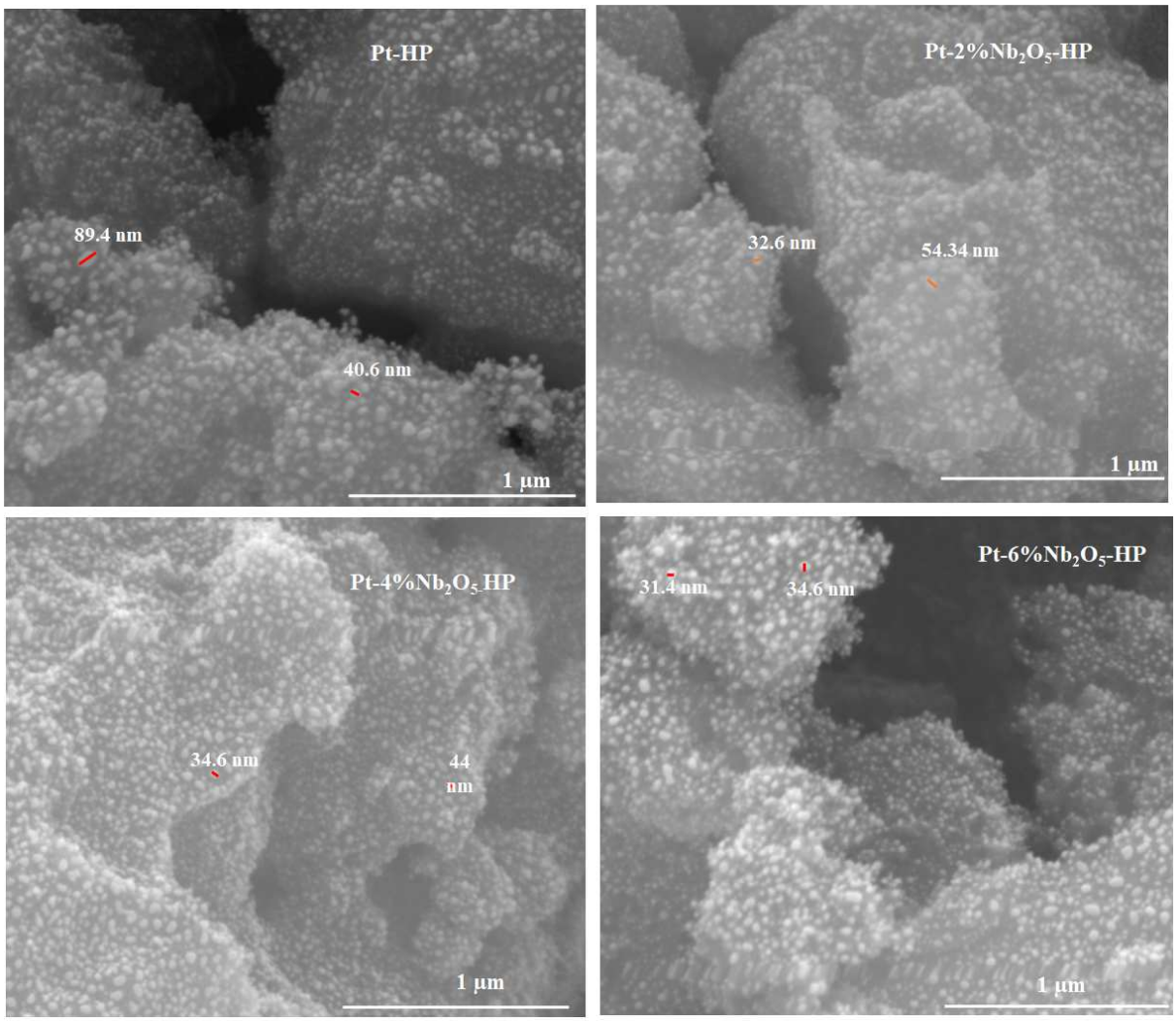

Fig. 2. Selected SEM micrographs of the examined photocatalysts.

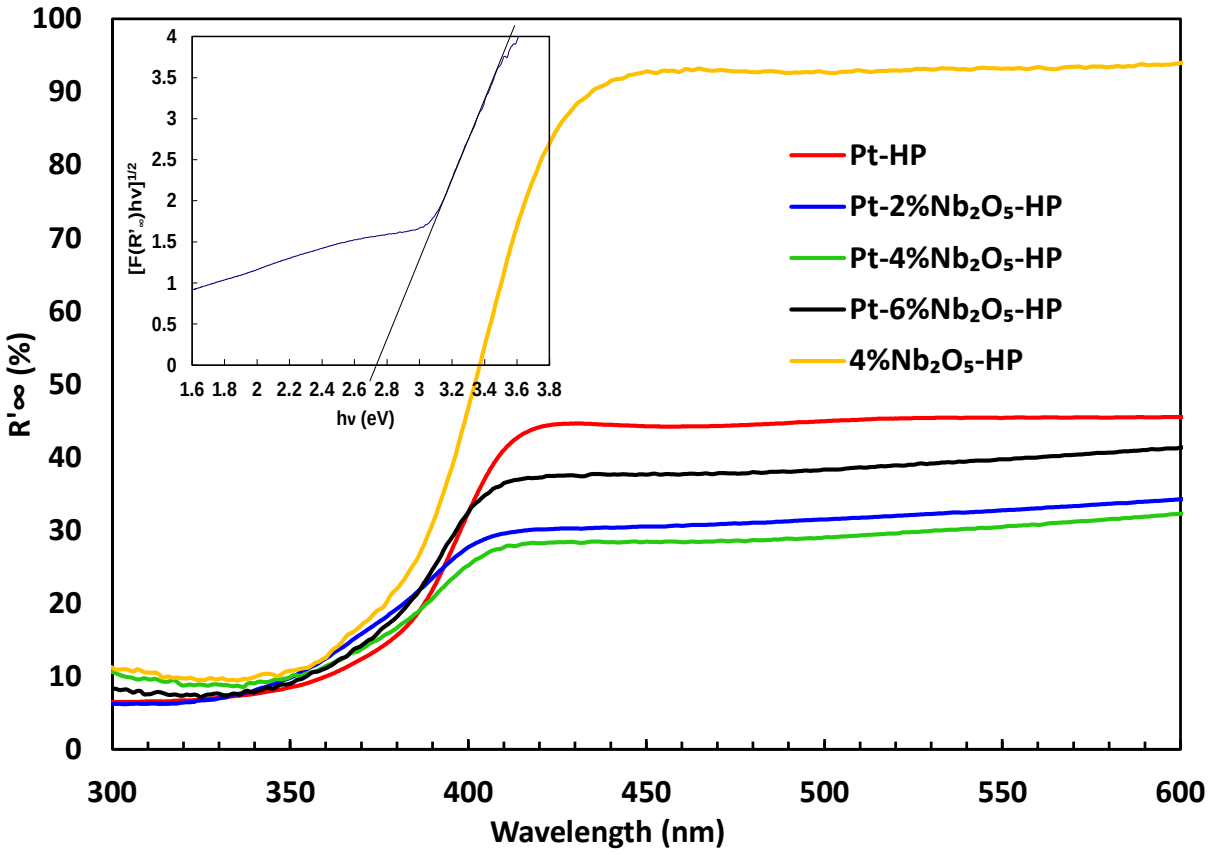

Fig. 3. UV-Vis DRS spectra of the prepared photocatalysts.

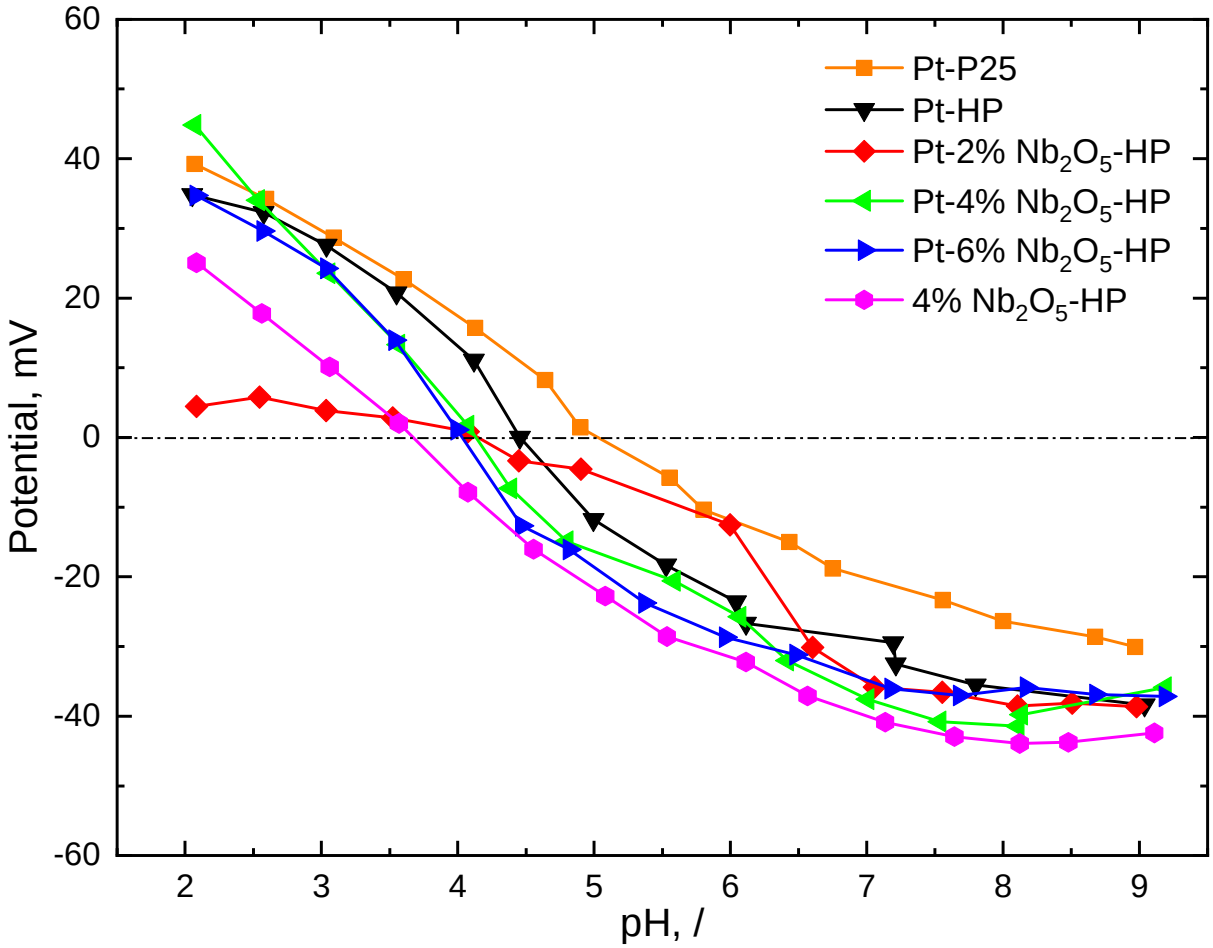

Fig. 4. Results of the pH related zeta potential measurements.

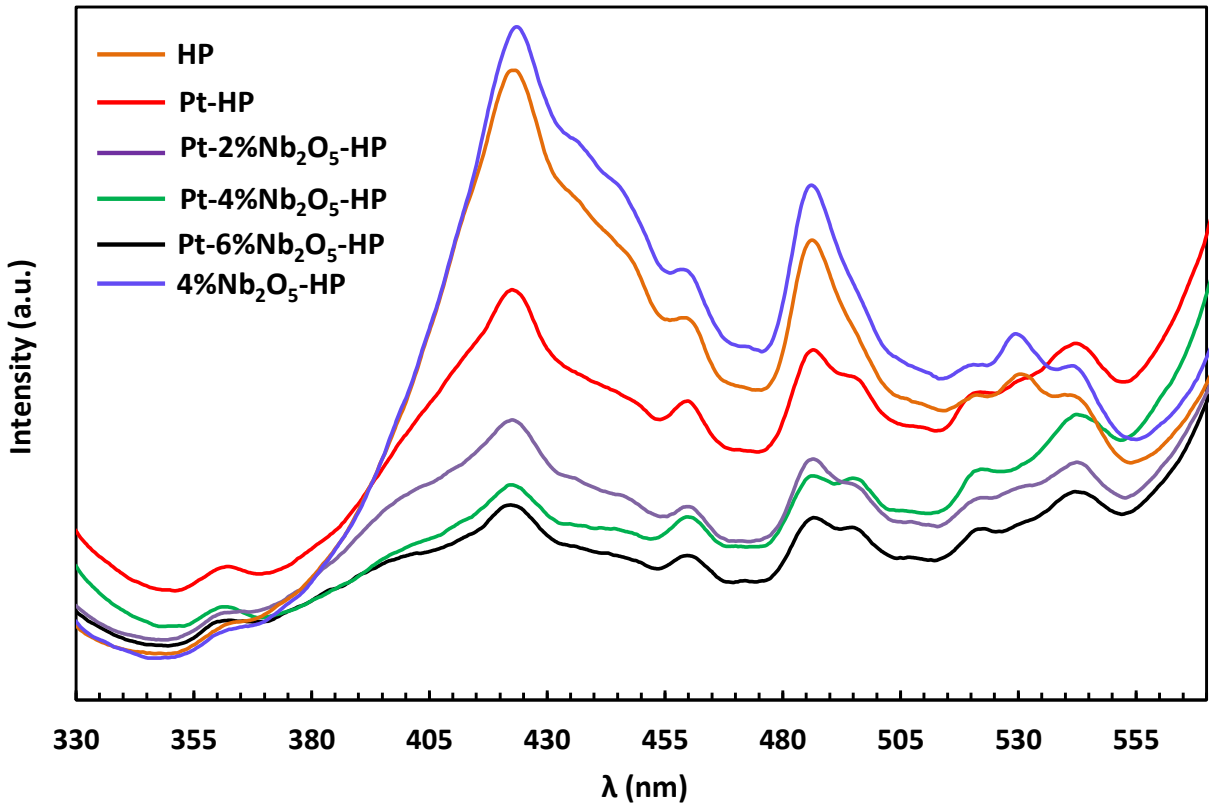

Fig. 5. Solid-state photoluminescence spectra of the different samples.

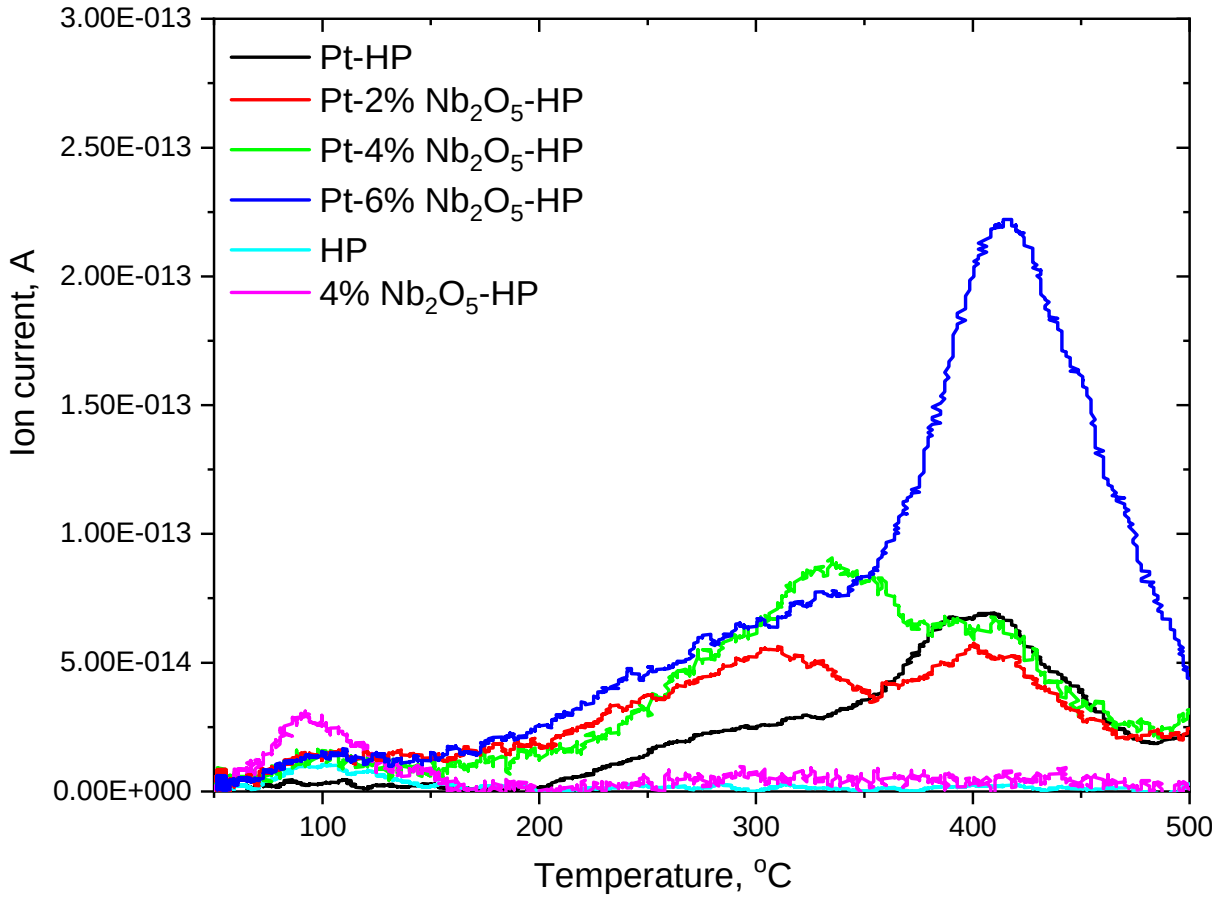

Fig. 6. CO_2 TPD curves of tested materials.

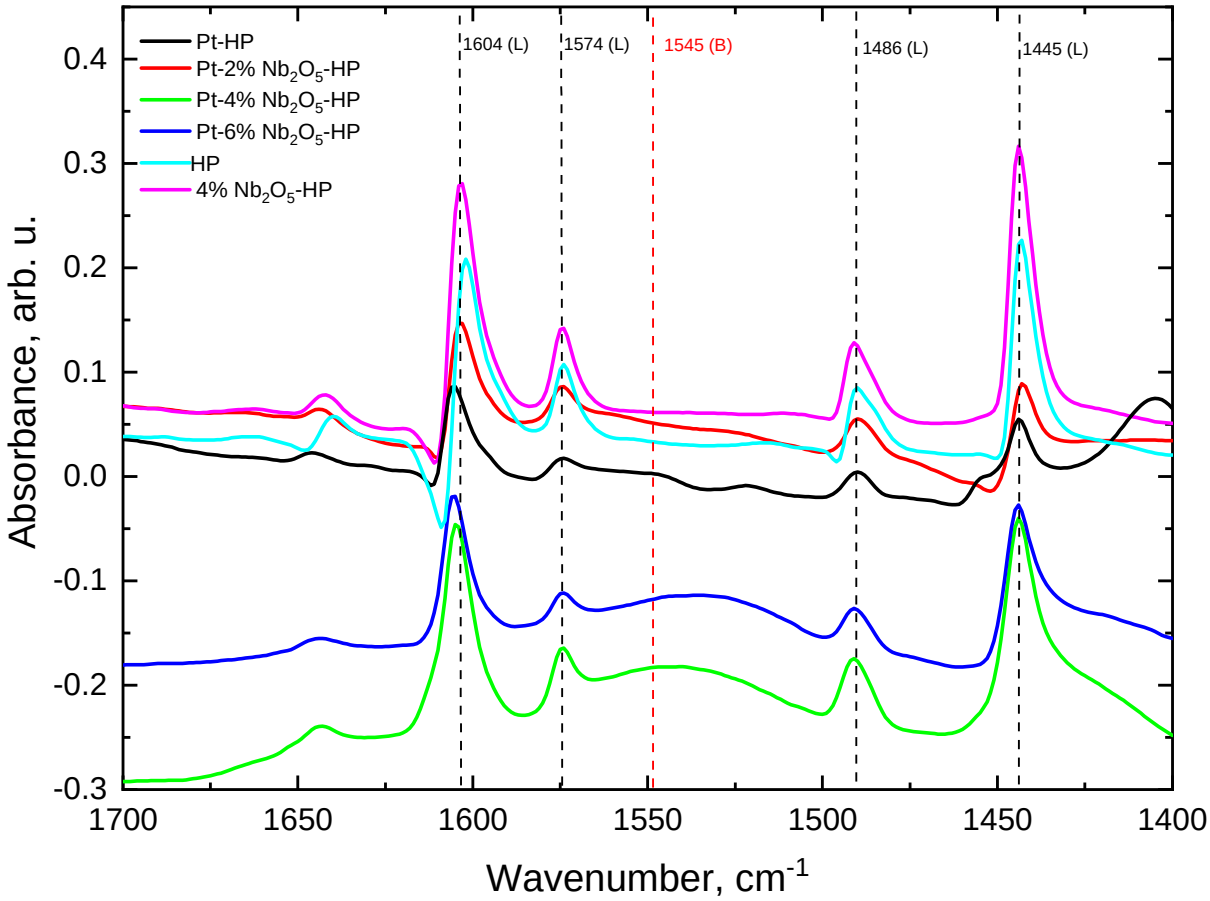

Fig. 7. DRIFTS spectra of pyridine adsorbed on the surface of investigated materials.

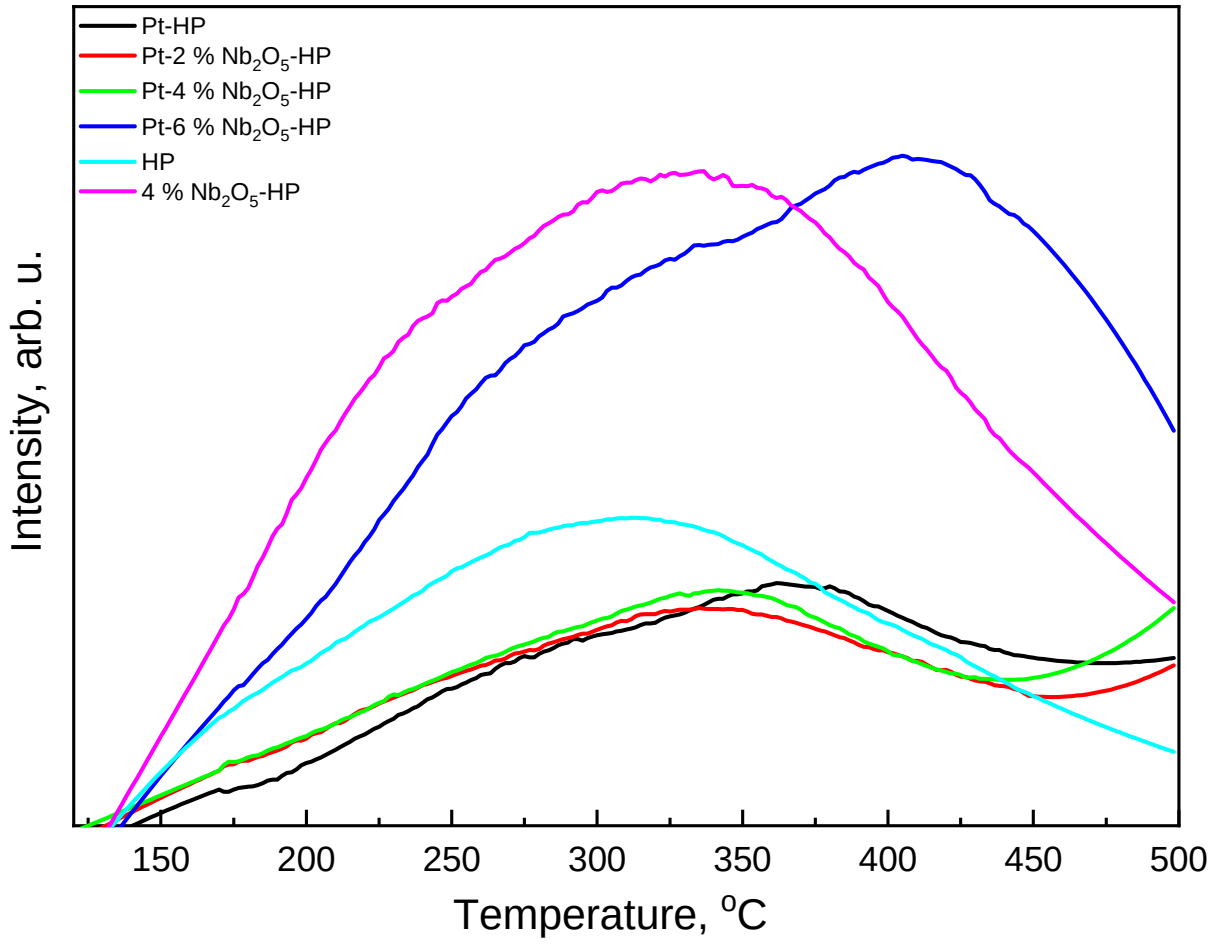

Fig. 8. Pyridine TPD curves for the investigated photocatalysts.

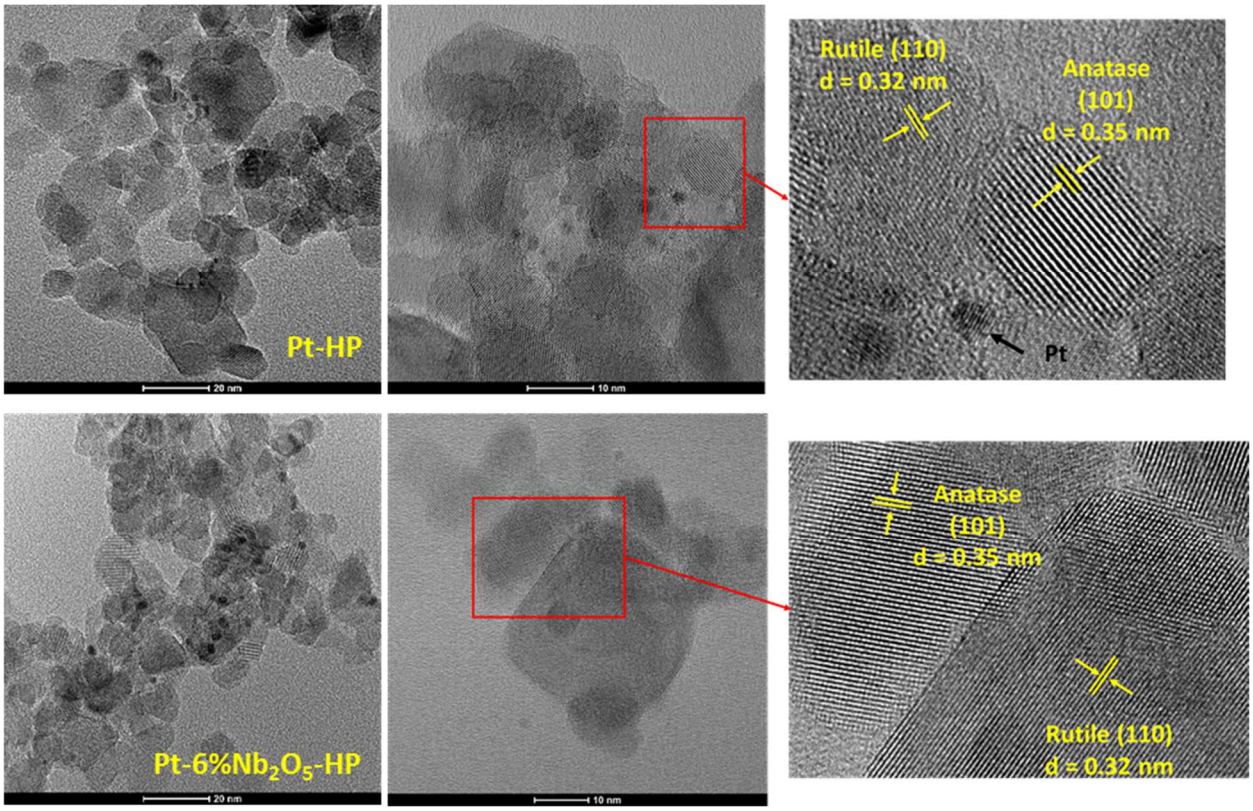

Fig. 9. TEM images of the Pt-HP and Pt-6%Nb_2O_5-HP samples.

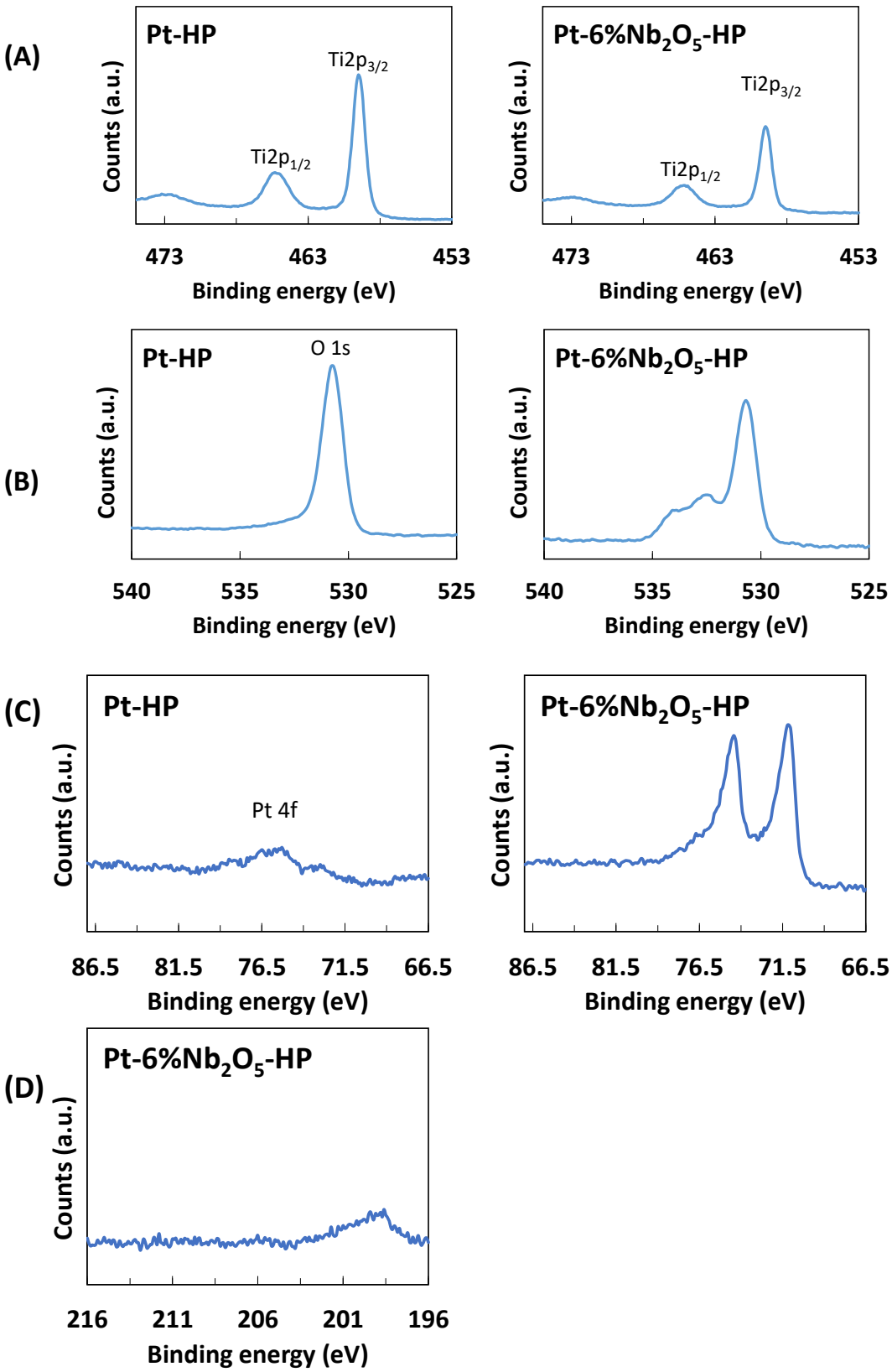

Fig. 10. High resolution XPS spectra of (A) Ti 2p, (B) O 1s, (C) Pt 4f, and (D) Nb 3d peaks.

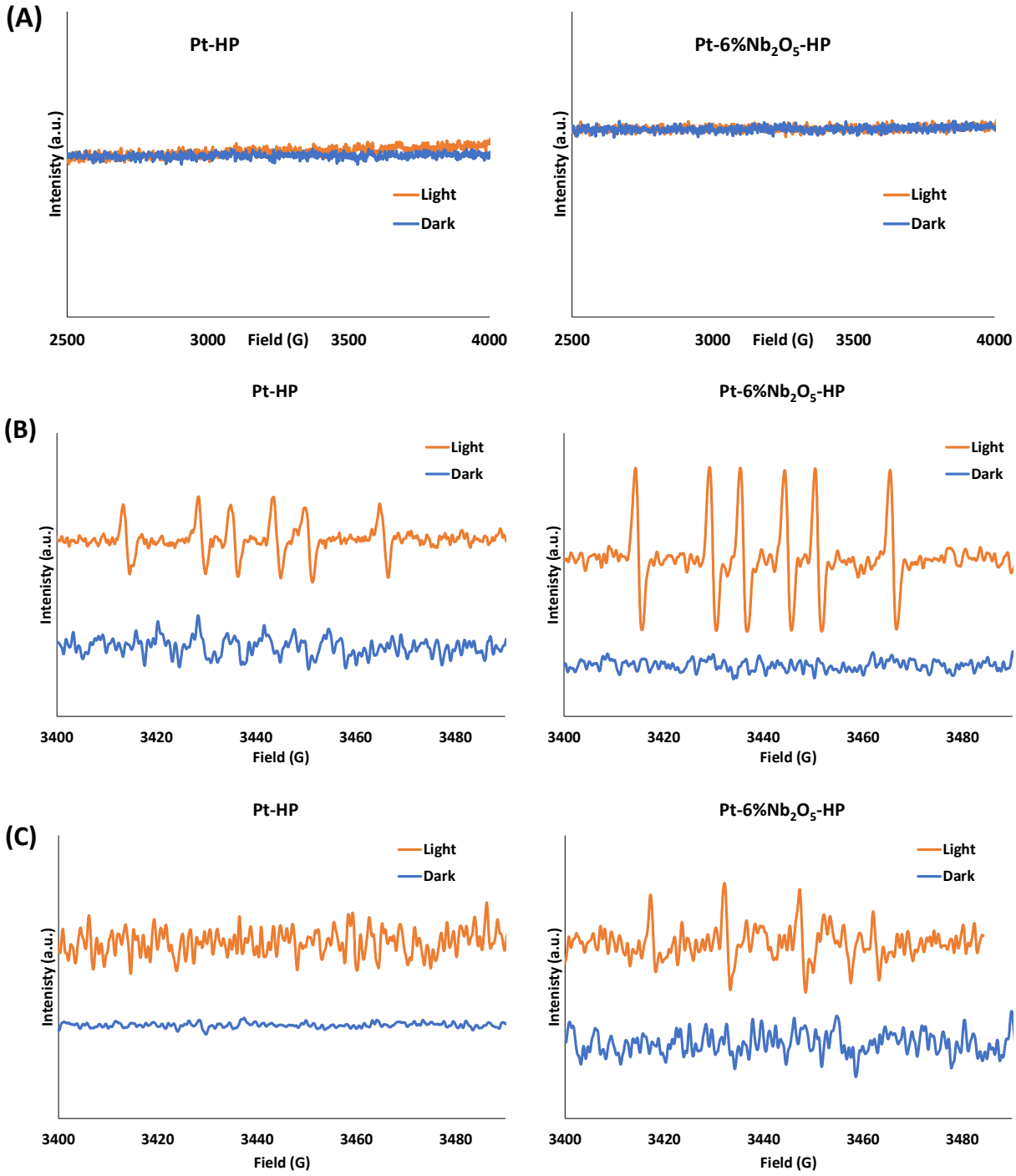

Fig. 11. EPR spectra of (A) powder samples Pt-HP and Pt-6%Nb_2O_5-HP under dark and light irradiation, (B) samples suspended in H_2O/DMPO/MeOH solution, and (C) samples suspended in H_2O/DMPO/H_2O_2 solution.

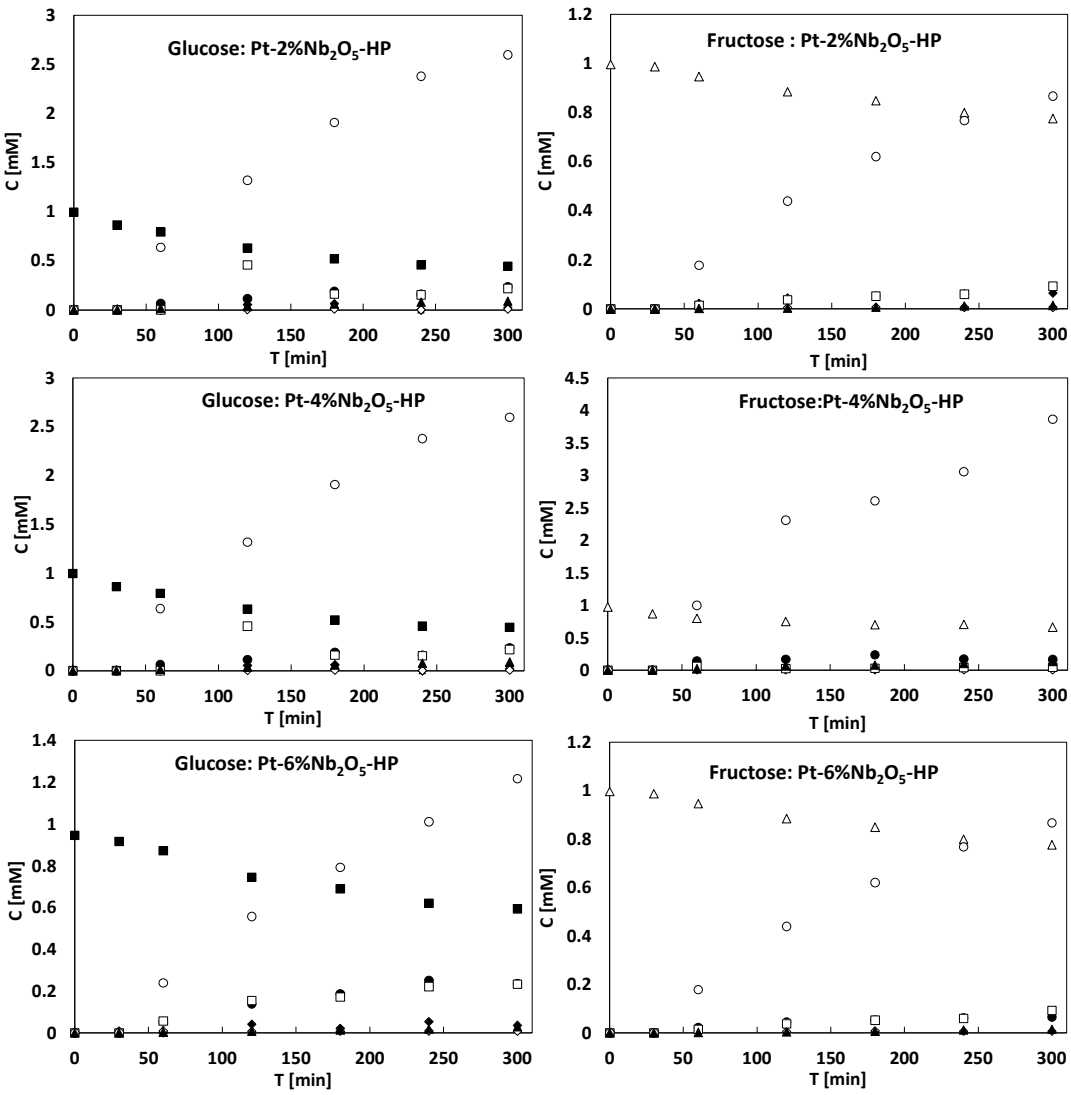

Fig. 12. Concentrations of the two substrates and their products versus irradiation time for runs carried out by using Nb_2O_5 modified photocatalysts. Legend: ■ glucose, Δ fructose, ● arabinose, ◇ gluconic acid, □ formic acid, ○ hydrogen, ▲ CO_2.

Table 1. Some physico-chemical properties of the investigated photocatalysts.

Sample	Phase	S.S.A. ($m^2\ g^{-1}$)	Band gap (eV)	pH_{PZC}
Pt-P25	Anatase + Rutile	50	3.09	5.00
Pt-HP	Anatase + Rutile	78	3.05	4.45
Pt-2%Nb_2O_5-HP	Anatase + Rutile	75	3.08	4.16
Pt-4%Nb_2O_5-HP	Anatase + Rutile	92	3.07	4.13
Pt-6%Nb_2O_5-HP	Anatase + Rutile	100	3.08	4.03
4%Nb_2O_5-HP	Anatase + Rutile	90	2.99	3.67

Table 2. Amount and density of basic sites in the tested materials calculated by CO_2 TPD analyses.

Sample	Mass of used catalyst (g)	Area (A s)	Amount of basic sites (μmol/g)	Density of basic sites (μmol/m^2)
HP	0.0499	7.38×10^{-12}	12.8	0.164
Pt-HP	0.0520	5.74×10^{-11}	53.6	0.687
4%Nb_2O_5-HP	0.0461	2.15×10^{-11}	21.0	0.269
Pt-2%Nb_2O_5-HP	0.0565	8.37×10^{-11}	46.7	0.622
Pt-4%Nb_2O_5-HP	0.0508	1.0×10^{-10}	83.7	0.909
Pt-6%Nb_2O_5-HP	0.0479	1.85×10^{-10}	121	1.210

Table 3. Amount and density of acid sites and the corresponding temperature of pyridine desorption from the surface of different samples.

Sample	Amount of acid sites (mmol/g)	Density of acid sites (mmol/m^2)	T of pyridine desorption (°C)
HP	0.1605	0.0021	310
Pt-HP	0.1137	0.0015	375
4%Nb_2O_5-HP	0.2274	0.0029	331
Pt-2%Nb_2O_5-HP	0.1545	0.0021	341
Pt-4%Nb_2O_5-HP	0.1863	0.0020	341
Pt-6%Nb_2O_5-HP	0.2219	0.0022	331, 406

Table 4. Glucose conversion, selectivity towards the main products, and H_2 and CO_2 amounts obtained after 5 h of irradiation.

Sample	Conversion	Selectivity					H_2	CO_2
		Fructose	Gluconic acid	Arabinose	Formic acid	Erythrose		
		(%)						
	(%)						(mM)	(mM)
Pt-HP	40	27	2.6	45	44	-	1.9	0.14
Pt-2%Nb_2O_5-HP	56	4	1.2	42	39	3.5	2.6	0.09
Pt-4%Nb_2O_5-HP	43	-	1.0	54	39	5.0	3.4	0.10
Pt-6%Nb_2O_5-HP	41	-	1.8	58	57	9.0	1.2	0.03
4%Nb_2O_5-HP	22	-	3.4	53	44	-	-	0.01
Pt-P25	32	31	4.6	41	31		1.9	0.07

Table 5. Fructose conversion, selectivity towards the main products, and H_2 and CO_2 amounts obtained after 5 h of irradiation.

Sample	Conversion	Selectivity				H_2	CO_2
		Gluconic acid	Arabinose	Formic acid	Erythrose		
	(%)	(%)				(mM)	(mM)
Pt-HP	40	4.5	-	6	7.5	3.2	0.12
Pt-2%Nb_2O_5-HP	39	2.2	75	15	9	1.9	0.07
Pt-4%Nb_2O_5-HP	40	2.0	42	11	9	3.8	0.14
Pt-6%Nb_2O_5-HP	22	3.0	-	41	29	0.9	0.01
4%Nb_2O_5-HP	13	4.2	-	24	-	-	0.01
Pt-P25	25	9		12		3.13	0.10